BIOCHEMISTRY
including biophysical chemistry & molecular biology

Rapid Report

pubs.acs.org/biochemistry

Neurofibrillar Tangle Surrogates: Histone H1 Binding to Patterned Phosphotyrosine Peptide Nanotubes

Sha Li,[†] Anton N. Sidorov,[‡] Anil K. Mehta,[†] Anthony J. Bisignano,[†] Dibyendu Das,[†,§] W. Seth Childers,[†,∥] Erin Schuler,[†] Zhigang Jiang,[⊥] Thomas M. Orlando,[‡] Keith Berland,[†] and David G. Lynn*[,†]

[†]Departments of Chemistry, Biology, and Physics, Emory University, Atlanta, Georgia 30322, United States

[‡]School of Chemistry and Biochemistry, [⊥]School of Physics, Georgia Institute of Technology, Atlanta, Georgia 30332, United States

Supporting Information

ABSTRACT: Living cells contain a range of densely phosphorylated surfaces, including phospholipid membranes, ribonucleoproteins, and nucleic acid polymers. Hyperphosphorylated surfaces also accumulate in neurodegenerative diseases as neurofibrillar tangles. We have synthesized and structurally characterized a precisely patterned phosphotyrosine surface and establish this assembly as a surrogate of the neuronal tangles by demonstrating its high-affinity binding to histone H1. This association with nucleic acid binding proteins underscores the role such hyperphosphorylated surfaces may play in disease and opens functional exploration into protein−phosphorylated surface interactions in a wide range of other complex assemblies.

Tauopathies, including Alzheimer's disease (AD) and Pick's disease, are characterized by the cytoplasmic accumulation of densely phosphorylated neurofibrillar tangles of the microtubule-associated tau protein.[1−3] The recent identification of specific ribonucleoprotein colocalization with hyperphosphorylated tau aggregates implies that co-aggregation or even cross-seeding events may be etiologically significant in AD by impacting RNA processing.[4] Here we use the paracrystalline phase of the Aβ peptide to develop a neurofibrillar tangle surrogate with a precisely patterned phosphopeptide surface and use it to evaluate histone H1 binding.

Aβ(16−22), Ac-KLVFFAE-NH_2,[5] and its congener, Ac-KLVFFAL-NH_2 (E22L), assemble as peptide bilayer nanotubes[6,7] (Figure 1A) with diameters of 54 ± 3[6] and 32 ± 5 nm, respectively (Figure S1 of the Supporting Information). The peptides in each leaflet of the peptide bilayer are arrayed as β-sheets having antiparallel out-of-register strand arrangements, placing the N-terminal residues outside the H-bonded array.[6] The positively charged lysine side chains are in rows running the length of the tube and repeat every nanometer on each leaflet face.[6]

Reasoning that these robust, β-sheet rich, cross-β peptide assemblies might also accommodate phosphorylated residues along the leaflet surface, we synthesized the phosphotyrosine Ac-(pY)LVFFAL-NH_2 peptide (K16pY)(E22L) and found conditions (40% MeCN/H_2O mixture and 15 mM triethylammonium acetate at neutral pH) under which nanotubes assemble with diameters of 32 ± 3 nm (Figure 1E and Figure S1 of the Supporting Information).

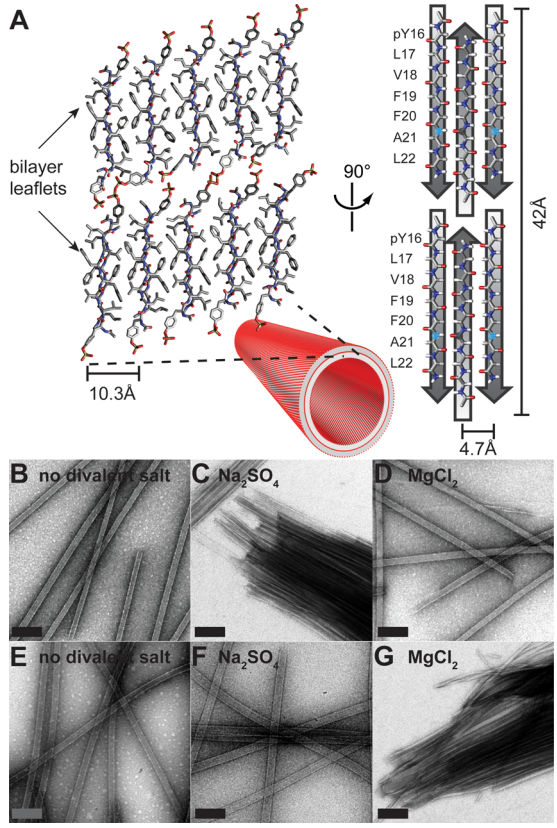

Figure 1. (A) Model for (K16pY)(E22L) bilayer nanotubes with each leaflet composed of antiparallel out-of-register β-sheets. The N-terminal phosphotyrosine (pY) repeats every nanometer along each row. (B−G) Transmission electron microscopy micrographs of salt-induced bundling of (E22L) (top) and (K16pY)(E22L) (bottom) nanotubes: (B and E) without additional salts, (C and F) 2 h after the addition of Na_2SO_4, and (D and G) 2 h after the addition of $MgCl_2$. Peptide:salt molar ratio of 1:4.5 and scale bars of 200 nm.

The (K16pY)(E22L) nanotubes exhibit a circular dichroism (CD) ellipticity minimum at 225 nm (Figure S2 of the Supporting Information), most consistent with β-sheets.[8] Powder X-ray diffraction (XRD) reflections with *d* spacings of

Received: May 18, 2014
Revised: June 17, 2014
Published: June 23, 2014

4.7 and 10.3 Å (Figure S3 of the Supporting Information) can be assigned as β-strand and β-sheet reflections, respectively, within a cross-β assembly.[6,9−14] Fourier transform infrared spectra (Figure S4 of the Supporting Information) contain a strong amide I absorption band at 1623 cm^{-1}, further supporting H-bonded β-sheet structures, and a weak band at 1693 cm^{-1} consistent with antiparallel strand arrangements.[6] The out-of-register antiparallel organization is confirmed via solid-state nuclear magnetic resonance (NMR) $^{13}C\{^{15}N\}$REDOR[15] measurements on [1-^{13}C]V18,[^{15}N]A21-(K16pY)(E22L) assemblies, assigning Val18 as H-bonded to Ala21 on adjacent strands with $^{13}C-^{15}N$ distances of 4.2 ± 0.2 and 5.8 ± 0.2 Å and a $^{15}N-^{13}C-^{15}N$ angle of 156° (Figure S5 of the Supporting Information), identical to Aβ(16−22) and (E22L) tubes.[6] As shown in Figure 2 (left), atomic force microscopy (AFM)

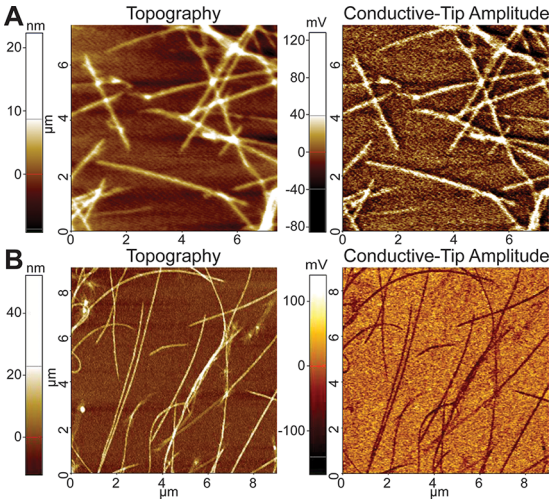

Figure 2. Atomic and electrostatic force micrographs of (A) (E22L) and (B) (K16pY)(E22L) nanotube assemblies. Topography (left) and EFM amplitude (right) micrographs of peptide nanotubes with a DC bias of +1 V. In the EFM amplitude micrographs, positively charged surfaces are white and negatively charged surfaces darker.

(Figure S6 of the Supporting Information) measurements are consistent with E22L and (K16pY)(E22L) tubes each maintaining the ∼4 nm thick wall of a cross-β peptide bilayer.[7] The antiparallel β-sheet registry then places the phosphorylated residues on inner and outer tube surfaces and within the bilayer interface, establishing that this peptide bilayer is indeed capable of accommodating polar phosphates at the leaflet interface (Figure 1A).

Salt-induced[16] aggregation was used to evaluate the nanotube surface charge. Induction follows the Hofmeister series,[17,18] with SO_4^{2-} bundling (E22L) nanotubes[18] but not (K16pY)(E22L) nanotubes (Figure 1C,F), consistent with (E22L) having positively charged surfaces and (K16pY)(E22L) having negatively charged surfaces. Similarly, Mg^{2+} bundles only (K16pY)(E22L) nanotubes (Figure 1D,G). Further, citrate-coated negatively charged gold nanoparticles organize specifically along the surfaces of the (E22L) assemblies, while positively charged gold nanoparticles [functionalized with (11-mercaptoundecyl)-*N*,*N*,*N*-trimethylammonium bromide] coat only the (K16pY)(E22L) assemblies (Figure S7 of the Supporting Information). Together, these results are consistent with (K16pY)(E22L) nanotubes having negatively charged surfaces and (E22L) nanotubes having positively charged surfaces.

Enhanced electrostatic force microscopy (EFM) supports these assignments and allows mapping of the charge distribution, as with other peptide assemblies[19,20] and doped regions in semiconductors.[21,22] Figure 2A shows the partially dried (E22L) assemblies as repulsive (white) to a positive bias tip, while the (K16pY)(E22L) assemblies (Figure 2B) are attractive (dark) along the entire length of each assembled nanotube. These electrochemical potential measurements precisely map the assembled phases, and the analysis appears to be independent of counterion as the same EFM images are obtained with gold nanoparticles (data not shown) and protein (Figure S8 of the Supporting Information). Together, these spectroscopic and scanning probe analyses define a unique hyperphosphorylated peptide nanotube.

Histone H1 accumulates in the cytoplasm of neurons and astrocytes in areas impacted by neurodegenerative disease[23] and serves as a prototypical nucleic acid binding protein for initial evaluation of our new phosphorylated nanotube surfaces. The addition of histone H1 to (K16pY)(E22L) nanotubes does not disrupt the assemblies as visualized by transmission electron microscopy (TEM) (Figure 3A), and two-photon fluorescence

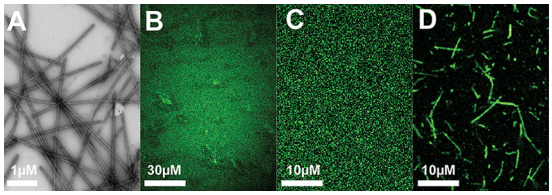

Figure 3. (A) TEM image of 500 μM (K16pY)(E22L) nanotube assemblies in the presence of 4.6 μM histone H1−Alexa 488 conjugate. (B−D) Single slices of the two-photon fluorescence image excited at 780 nm of 4.6 μM Alexa 488-labeled calf thymus histone H1 alone (B), in the presence of 500 μM E22L nanotube assemblies (C), and in the presence of 500 μM (K16pY)(E22L) nanotube assemblies (D).

images in Figure 3 show Alexa 488 fluorophore-labeled calf thymus histone H1 specifically sequestered by the negatively charged (K16pY)(E22L) nanotubes (Figure 3D), but not the positively charged (E22L) tubes (Figure 3C).

Isothermal titration calorimetry (ITC) thermograms show minimal heat change (Figure S9 of the Supporting Information) between histone H1 and (E22L) assemblies. In contrast, the addition of histone to (K16pY)(E22L) nanotubes (Figure S10 of the Supporting Information) fit to a one-site model with a large endothermic heat of binding (ΔH = 36.7 ± 5 kcal/mol) and a $-T\Delta S$ of −48 kcal/mol. This entropically driven association, with a K_a of (2.09 ± 0.3) × 10^8 M^{-1}, is remarkably 2 orders of magnitude higher than that of binding to calf thymus DNA at the same temperature.[24,25] Even more significantly, the saturation stoichiometry of (6.78 ± 0.06) × 10^{-3} binding sites per peptide translates into 147 ± 13 peptides per histone binding site.

A binding site of 147 peptides represents an area of 11.3 nm × 5.2 nm (59 nm^2) on the nanotube surface, a large area for a 2.9 nm diameter globular protein with short unstructured N- and C-termini.[26] To confirm the histone binding ITC values, fluorescence polarization (FP) is followed as (K16pY)(E22L) nanotubes are titrated into a fixed histone H1−Alexa 488 concentration (Figure S11 of the Supporting Information). Assuming noncooperative association and 147 peptides per binding site, the K_d of (4.8 ± 2.9) × 10^{-9} M is identical to the K_d determined by ITC [(4.78 ± 0.58) × 10^{-9} M]. A recent evaluation of the binding of histone H1 to DNA identifies a

dx.doi.org/10.1021/bi500599a | *Biochemistry* 2014, 53, 4225−4227

binding site of 32 ± 1 bp,[24] consistent with a histone length of 11 nm. With the 2.9 nm diameter of the globular domain, the histone coverage area can be estimated to be 11 nm × 3 nm (33 nm^2), on the order of the surface area calculated for binding to the (K16pY)(E22L) nanotube surfaces and consistent with significant conformational plasticity upon binding.

The eukaryotic cell matrix presents a labyrinth of phospholipid membranes partitioning diverse compartments in a sea of ribonucleoproteins, phosphorylated metabolites, and nucleic acid polymers. Such charged surfaces must all be navigated by the information processing cellular proteins that process nucleic acids. Association of histone H1 with the DNA backbone[27] is important in gene regulation,[28] chromatin condensation,[29] and global control over chromatin remodeling activities.[30] However, H1 also permeates biological membranes and has been used to chaperone chimeric macromolecules across cell barriers,[31] highlighting the range of phosphorylated surfaces on which this protein functions.

The synthetic accessibility and morphological tractability of these patterned peptide surfaces[5,6] now open entirely new possibilities for studying protein associations. For example, given that histone H1 was the first nucleic acid binding protein to be identified as mislocalized in amyloid diseases[23] and the recent implications of accumulation of other information processing proteins in disease plaques,[32] this neurofibrillar tangle surrogate can be used for proteomic screening of AD tissues and other aberrant cellular assemblies and exploration of seeding and co-assembly in disease etiology.[4]

■ ASSOCIATED CONTENT

Supporting Information

Details of synthesis, assembly, CD, XRD, IR, AFM, NMR, ITC, and FP of histone binding. This material is available free of charge via the Internet at http://pubs.acs.org.

■ AUTHOR INFORMATION

Corresponding Author

*E-mail: david.lynn@emory.edu.

Present Addresses

[§]D.D.: Institute of Nano Science and Technology (INST), Habitat Centre, phase-X, Sector 64, Mohali 160 062, India.

[∥]W.S.C.: Department of Developmental Biology, Stanford University School of Medicine, Stanford, CA 94305.

Funding

Supported by the Division of Chemical Sciences, Geosciences, and Biosciences, Office of Basic Energy Sciences of the U.S. Department of Energy, through Grant DE-ER15377, and the NASA Astrobiology Program, under the National Science Foundation Center for Chemical Evolution (CHE-1004570 and NSF-CBC-0739189).

Notes

The authors declare no competing financial interests.

■ ACKNOWLEDGMENTS

We thank the Robert P. Apkarian Microscopy Core of Emory University for TEM training and data collection, the Emory X-ray Center for powder diffraction, and Prof. Stephan Lutz of Emory University for fluorometer access.

■ REFERENCES

(1) Alonso, A. d. C., Zaidi, T., Novak, M., Grundke-Iqbal, I., and Iqbal, K. (2001) *Proc. Natl. Acad. Sci. U.S.A. 98*, 6923−6928.

(2) Inoue, M., Konno, T., Tainaka, K., Nakata, E., Yoshida, H.-o., and Morii, T. (2012) *Biochemistry 51*, 1396−1406.

(3) Williams, D. R. (2006) *Intern. Med. J. 36*, 652−660.

(4) Bai, B., Hales, C. M., Chen, P. C., Gozal, Y., Dammer, E. B., Fritz, J. J., Wang, X., Xia, Q., Duong, D. M., Street, C., Cantero, G., Cheng, D., Jones, D. R., Wu, Z., Li, Y., Diner, I., Heilman, C. J., Rees, H. D., Wu, H., Lin, L., Szulwach, K. E., Gearing, M., Mufson, E. J., Bennett, D. A., Montine, T. J., Seyfried, N. T., Wingo, T. S., Sun, Y. E., Jin, P., Hanfelt, J., Willcock, D. M., Levey, A., Lah, J. J., and Peng, J. (2013) *Proc. Natl. Acad. Sci. U.S.A. 110*, 16562−16567.

(5) Childers, W. S., Anthony, N. R., Mehta, A. K., Berland, K. M., and Lynn, D. G. (2012) *Langmuir 28*, 6386−6395.

(6) Mehta, A. K., Lu, K., Childers, W. S., Liang, Y., Dublin, S. N., Dong, J., Snyder, J. P., Pingali, S. V., Thiyagarajan, P., and Lynn, D. G. (2008) *J. Am. Chem. Soc. 130*, 9829−9835.

(7) Childers, W. S., Mehta, A. K., Ni, R., Taylor, J. V., and Lynn, D. G. (2010) *Angew. Chem., Int. Ed. 49*, 4104−4107.

(8) Hamley, I. W., Nutt, D. R., Brown, G. D., Miravet, J. F., Escuder, B., and Rodriguez-Llansola, F. (2010) *J. Phys. Chem. B 114*, 940−951.

(9) Astbury, W. T., Dickinson, S., and Bailey, K. (1935) *Biochem. J. 29*, 2351−2360.

(10) Parker, K. D., and Rudall, K. M. (1957) *Nature 179*, 905−906.

(11) Eanes, E. D., and Glenner, G. G. (1968) *J. Histochem. Cytochem. 16*, 673−677.

(12) Geddes, A. J., Parker, K. D., Atkins, E. D. T., and Beighton, E. (1968) *J. Mol. Biol. 32*, 343−358.

(13) Inouye, H., Fraser, P. E., and Kirschner, D. A. (1993) *Biophys. J. 64*, 502−519.

(14) Sunde, M., and Blake, C. C. (1998) *Q. Rev. Biophys. 31*, 1−39.

(15) Gullion, T., and Schaefer, J. (1989) *J. Magn. Reson. 81*, 196−200.

(16) Sadeghi, R., and Jahani, F. (2012) *J. Phys. Chem. B 116*, 5234−5241.

(17) Hofmeister, F. (1888) *Arch. Exp. Pathol. Pharmakol. 24*, 247−260.

(18) Lu, K., Guo, L., Mehta, A. K., Childers, W. S., Dublin, S. N., Skanthakumar, S., Conticello, V. P., Thiyagarajan, P., Apkarian, R. P., and Lynn, D. G. (2007) *Chem. Commun.*, 2729−2731.

(19) Lee, G., Lee, W., Lee, H., Lee, S. W., Yoon, D. S., Eom, K., and Kwon, T. (2012) *Appl. Phys. Lett. 101*, 043703−043704.

(20) Clausen, C. H., Dimaki, M., Panagos, S. P., Kasotakis, E., Mitraki, A., Svendsen, W. E., and Castillo-Leon, J. (2011) *Scanning 33*, 201−207.

(21) Gomez, A., Avila, A., and Hinestroza, J. P. (2010) *J. Electrost. 68*, 79−84.

(22) Bonilla, R., Avila, A., Montenegro, C., and Hinestroza, J. (2012) *J. Microsc. 248*, 266−270.

(23) Duce, J. A., Smith, D. P., Blake, R. E., Crouch, P. J., Li, Q.-X., Masters, C. L., and Trounce, I. A. (2006) *J. Mol. Biol. 361*, 493−505.

(24) Machha, V. R., Jones, S. B., Waddle, J. R., Le, V. H., Wellman, S., and Lewis, E. A. (2014) *Biophys. Chem. 185*, 32−38.

(25) Xiao, B., Freedman, B. S., Miller, K. E., Heald, R., and Marko, J. F. (2012) *Mol. Biol. Cell 23*, 4864−4871.

(26) Dootz, R., Toma, A. C., and Pfohl, T. (2011) *Biomicrofluidics 5*, 24104.

(27) Graziano, V., Gerchman, S. E., Schneider, D. K., and Ramakrishnan, V. (1994) *Nature 368*, 351−354.

(28) Dou, Y. L., Mizzen, C. A., Abrams, M., Allis, C. D., and Gorovsky, M. A. (1999) *Mol. Cell 4*, 641−647.

(29) Roth, S. Y., and Allis, C. D. (1992) *Trends Biochem. Sci. 17*, 93−98.

(30) Horn, P. J., Carruthers, L. M., Logie, C., Hill, D. A., Solomon, M. J., Wade, P. A., Imbalzano, A. N., Hansen, J. C., and Peterson, C. L. (2002) *Nat. Struct. Biol. 9*, 263−267.

(31) Hariton-Gazal, E., Rosenbluh, J., Graessmann, A., Gilon, C., and Loyter, A. (2003) *J. Cell Sci. 116*, 4577−4586.

(32) Dammer, E. B., Duong, D. M., Diner, I., Gearing, M., Feng, Y., Lah, J. J., Levey, A. I., and Seyfried, N. T. (2013) *J. Proteome Res. 12*, 3193−3206.